Accepted Manuscript

Residual strength and damage characterization of repaired glass/epoxy composite laminates using A.E. and D.I.C

J. Jefferson Andrew, V. Arumugam, D.J. Bull, H.N. Dhakal

Please cite this article as: Jefferson Andrew, J., Arumugam, V., Bull, D.J., Dhakal, H.N., Residual strength and damage characterization of repaired glass/epoxy composite laminates using A.E. and D.I.C, *Composite Structures* (2016), doi: http://dx.doi.org/10.1016/j.compstruct.2016.05.005

Residual strength and damage characterization of repaired glass/epoxy composite laminates using A.E. and D.I.C.

[a]J. Jefferson Andrew, [a]V. Arumugam, [b]D. J. Bull, [c]*H.N. Dhakal

[a] Department of Aerospace Engineering, Madras Institute of Technology, Anna University, Chennai, India

[b]Faculty of Engineering and the Environment, University of Southampton, Southampton, SO17 1BJ, UK

[c]Advanced Polymer and Composites (APC) Research Group, School of Engineering, University of Portsmouth, Anglesea Road, Anglesea Building, Portsmouth, Hampshire PO1 3DJ, UK

Abstract:

In this paper, the effect of introducing different phases of fibre reinforcement in epoxy matrix at the dressed site in adhesively bonded external patch repair for damaged glass/epoxy composites under in-plane compressive loads was investigated. Three repair materials consisting of an epoxy matrix reinforced with either micro sized particulate fibres, chopped short fibres or continuous fibres were used in this study. Since this investigation extensively focuses on the effect of different types of fibre reinforcements on residual compression properties of repaired glass/epoxy composite laminates, the external patches were avoided. Acoustic Emission (AE) and Digital Image Correlation (DIC) were utilized to form qualitative and quantitative assessments of the damage progression profile. The compression results illustrate that reinforcing the epoxy adhesive material with glass fibres significantly increased the residual compression strength of repaired glass/epoxy composite specimens. In particular, the use of chopped fibre reinforced adhesive repair material improved the average residual compressive strength by 18.91 % in comparison to the specimens conventionally repaired using neat epoxy resin.

* Corresponding author. Tel: + 44 (0) 23 9284 2582; fax: + 44 (0) 23 9284 2351.

E-mail: hom.dhakal@port.ac.uk

1. Introduction

Fibre reinforced composite laminates are extensively used in lightweight, high performance, safety relevant structural applications due to their high stiffness to weight and strength to weight ratios. Nowadays, laminated composites are replacing traditional materials like aluminum and steel owing to their high fatigue resistance, corrosion resistance, tailorability and repairability. However, the mechanical strength, durability and reliability offered by composites are affected by their poor damage tolerance to transient loading [1] and minor manufacturing defects like voids [2]. Low velocity impact damage like interlaminar delamination, fibre splitting, matrix cracking and fibre breakage can significantly reduce the residual strength and stiffness of composite laminates [3]. Also, catastrophic failure of the entire system may take place due to consequent usage of the damaged structure in service.

To restore the structural integrity of a damaged component, the damaged area should be repaired or the entire damaged component should be replaced. The choice of replacement or repair of the damaged component relies on several factors, such as the location of damage on the structure, thickness, aerodynamic requirements, operation conditions: pressure, temperature and moisture, weight, mechanical property requirements and the damage area or extent of damage [4]. Due to costs of replacement parts, the repair of damaged components is often preferred [5]. Damage in composite laminates needs to be exactly assessed to carry out a suitable repair procedure. The maximum size and other limits for a adhesively bonded external patch repair depend on the constraints inherent in the design to be repaired, which means that the maximum size is defined one at a time relying on the type of aircraft (design, among others) and damage zone. Nothing can standardize, but in each case the maximal surface or diameter is a main and strategic parameter. There may also be repair size limits or other limitations related with substantiating data employed to meet appropriate rules. All critical structure will have a repair size limit no larger than a size that allows limit load strength to be achieved with the repair failed or failed within constrains of the arresting design features. The efficiency of a repair technique depends on the quality of dressing the damaged site, safety to cost ratio, durability and the stress intensity factor produced around the dressed region [6]. The initial step in the repair process of a damaged composite laminate is to dress the damaged region (originally irregular area) to provide it an evenly curving boundary, e.g. producing round border. This pace alone enhances the stress pattern in the laminate around the hole. The region in the parent laminate where the original irregular damage area is smoothened is termed as dressed site or dressed region [7]. Fastener and adhesive bonded repairs are the two most commonly practiced repair techniques in composite laminates [6]. Compared to fastener repair, adhesive bonded repairs have outstanding benefits such as low stress concentration, less weight and better formability. The methods in adhesive bonded repair include: scarf repair and patch repair [8]. The procedure for patch repair is relatively easy compared with scarf repair which necessitates careful machining to produce a required taper angle without damaging the surrounding area and bottom plies, and is particularly

difficult on curved surfaces. Thus, the adhesive bonded patch repair is often preferred when repairing a curved surface [6].

Much of the experimental and numerical research work to date concerning patch repair have focused on shape, thickness, orientation and overlap length of the external patches [9-10], whilst little attention has been given to the repair material used for filling the dressed area. At present, the dressed region in parent composite laminate is mostly filled using homogeneous pure resin [11]. However, under various service loads the efficiency of an adhesively bonded external patch repaired laminate depends not only on the shape, orientation and thickness of the external patches, but also on the stiffness of the material used to fill the dressed region; therefore, to ensure better performance, a filler material with higher stiffness must be introduced. It has been illustrated elsewhere that filling the cutout with appropriate materials on the repaired specimen, can have a favorable influence on repair performance [12]. Soutis et al [12] reported that the incorporation of an appropriate filler material in the cutout lessens the stress concentration factor, leading to higher residual mechanical strength (80–90% of the virgin or normal value). They investigated the influence of filler material (i.e. adhesive plugs) of varying stiffness on stress concentration. Filling the open cutout is revealed to decrease the stress concentration at the free edges of the hole and further enhance the residual strength by local stiffening relying on the type of the material. Furthermore, they studied the effect of plug stiffness and patch thickness on the compression behaviour of adhesively bonded external patch repaired carbon/epoxy specimens. They reported that patch thickness appears to have no considerable influence on the residual strength but the incorporation of the plug with optimum stiffness can increase the ultimate load of the repair configuration by around 20 %. The finite element analysis results reveals that for specimens repaired by incorporating appropriate plug in the dressed site the in-plane direct stress near the hole edge and the shear stress in the adhesive are much lesser than those of patch only repairs. Whilst these lower in-plane direct stress and shear stress result in a higher damage onset load, the repairs with a suitable filler material and thin patches will also offer a better constraint for damage progression. They showed that the value of SCF can reduce with increasing stiffness of the plug material. This would conclude that by optimizing stiffness of the plug material a residual tensile strength improvement of 10% can be obtained. They reported that materials like plastics, composites, metals can also be employed instead of adhesive plugs. For instance, reinforcing adhesives at the cutout with different fibre reinforcement can match the stiffness between the parent laminate and the repair material [13]. Hence, the selection of an appropriate adhesive reinforcement for matching stiffness requires a thorough understanding of ultimate strength, failure modes and damage propagation of the adhesive reinforced repaired specimens under mechanical loading.

Many researchers have reported numerical and experimental results on the quasi-static tensile and dynamic fatigue behaviour of adhesive bonded repair on fibre reinforced composite laminates [5, 11, 14]. On the other hand, only a few studies are available regarding the effects of an adhesive repair on residual compressive strength, and in particular the understanding of the

mechanisms leading to failure is not well understood [15, 16]. The combination of several failure modes like matrix cracking, fibre/matrix debonding, delamination, and fibre micro buckling can all influence the compressive strength of the laminate [12]. Many authors [17-19] used online AE monitoring techniques to qualitatively characterize the failure mode in composite laminates. When a composite laminate is strained, different damage modes are activated such that, a fraction of the whole strain energy is dissipated as a wave that transmitted from the damage source all the way through the medium. The consequential waves are called Acoustic Emissions which are dissipated owing to the onset of micro structural changes in the laminate. Acoustic Emissions transmit through the laminate until up to it reaches at a remote sensor. In reply, the sensor generates an electrical signal, which is transmitted to acquisition and processing equipment for further processing [20]. Acoustic emission techniques enable us to widen our hearing to sense sounds of lower intensities and higher frequencies. Hence acoustic emission monitoring technique is a good tool to detect the failure advancement in composite materials. Previous investigation on A.E. focused on correlating extracted features, such as amplitude and duration to failure. Events such as matrix cracking, fibre-matrix interfacial debonding, and fibre-break-up can be identified by a range of AE parameters, particularly amplitude and duration distribution [20]. The wavelet transformation is employed to process acoustic emission signals to obtain both time and frequencies information [21–23]. Fast Fourier Transform procedure (FFT), indicates the predominant frequencies, which are related to the major damage modes, while Short-Time Fast Fourier Transform analysis (ST-FFT) procedure provides the time information and thus the chronological events during failure process. Briefly, Spectrograms and ST-FFT's enable analyzing and visualizing the data in both a frequency and time domain at the similar time. This provides an outlook into how acoustic emission frequency content is changing at any specific time or point of the waveform.

Many literature can be found on acoustic emission amplitude-based discrimination. Berthelot and Rhazi [24] have investigated amplitude distribution of AE waveform from different tests on cross-ply and unidirectional composite laminates. They reveal that high amplitude waveforms are allied with fibre fracture and low amplitude waveforms with transverse matrix cracking and debonding. Wadim [25] associated a few ranges of amplitude to various damage mechanisms identified in organic matrix composites. He ascribed the low amplitude range (from 30 to 45 dB) to the resin or matrix cracking, then from 45 to about 55 dB (i.e. moderate amplitude ranges) to the interface debonding failure and lastly, beyond 55 dB to the fibre failure. Gong et al. [26] reported that AE signals with intermediate ranges are associated with friction of interface and the fibre pull-out damage. Kim and lee [27] reported that the low amplitude range (from 40 to 70 dB) to the resin or matrix cracking, and high amplitude range from 60 to about 100 dB to the fibre failure. Kotsikos [28] also reported that the low amplitude range (from 40 to 55 dB) to the resin or matrix cracking, then from 55 to about 70 dB to the interface debonding failure and beyond 70 dB to the fibre failure. Likewise, Mechraoui et al. [44] investigated AE wave propagation and velocity evolution in glass epoxy composites according to the fibre orientation. Their finding confirms that AE results obtained can be utilized to improve

AE testing on an industrial structure scale. Table 1 summaries failure mode links to AE amplitude proposed by different authors for glass fibre reinforced composites. Most of the authors tell contradictory amplitude ranges for various damage modes. However, it is frequently reported and well accepted in most of the literature that the AE signals with least amplitude ranges correspond to matrix or resin cracking, those with highest amplitude ranges correspond to fibre failure, and those with mid-amplitude ranges relate to delamination or fibre/matrix debonding damage modes.

Acoustic emission was globally used for online structural health monitoring, whilst it always requires a post NDT method, such as ultrasonic or X ray tomography, to quantify the extent of damage. Furthermore, the real time quantitative assessment of damage progression in repaired specimen is a challenging task. DIC technique can significantly reduce the complexity in characterizing the strain fields, strain zone shift, displacement field and damage propagation in composite laminates under mechanical loading. Failure investigation studies in repaired composite laminates were recently investigated using optical DIC technique. DIC technique gives a direct measure of displacements by comparing the images of loaded components with load free components [30]. Combining both the techniques (i.e. AE and DIC) assists in correcting the downsides in both of them; the difficulty in the interpretation of sound waves was made easy with the visual images and the difficulty in making use of the optical technique for practical, large-scale purposes. DIC technique is an advanced, non-contact, image based, full-field strain or displacement measurement technique capable of characterizing materials encountering mechanical, thermal, or various environmental loading [30 and 31]. The main advantage of the DIC technique compared to conventional NDT techniques is that it presents full-field strain and displacement data for numerous numbers of points for single specimen [32]. For uniform results, the strain fields may be additionally averaged to provide a statistical mean.

This paper investigates the compressive restoration effects of various phases of adhesive reinforcements (particulate fibres, chopped short fibres and continuous fibres) used to repair damaged glass/epoxy composite laminates. Furthermore, an extensive study was done to investigate the failure modes and damage progression of different repair configurations utilizing NDT monitoring comprising of AE and DIC techniques. Instantaneous damage progression and median longitudinal strain of the repaired laminates were observed using DIC and correlated with AE results.

2. Experimental procedure

2.1 Materials and Fabrication

The composite laminates of stacking sequence $(0/90/90/0)_{2s}$ were made up of unidirectional glass fabrics and epoxy resin (supplied by Marktech Composites, India) with sixteen laminas. Cross ply laminates of glass/epoxy were fabricated, as they (i.e. $(0/90/90/0)_{2s}$) offer superior resistance to crack propagation under in-plane compression load [33].Tables 2 and

3 shows the properties of the unidirectional glass fibre and the araldite epoxy resin, respectively. For fabricating fibre reinforced polymer laminate, fibres were reinforced into the resin system in a ratio of 1:1 by weight. The curing process was accelerated by adding a hardener (HY951) to the epoxy resin in a ratio of 1:10 by weight. The laminates were fabricated using conventional hand layup technique with a thicknesses of 4±0.125 mm and further cured under the aid of a 30 kN compression molding machine. In the compression molding machine, the laminates were cured under a pressure of 50 kg/cm^2 at room temperature (30ºC) for 24 hours. To maintain a uniform thickness of 4 mm throughout the laminate, a spacer plate of 4 mm was placed in-between the upper and lower mold of compression molding machine. To relieve the internal stresses due to molding pressure, the cured laminates were taken out from the compression molding machine and heated in an oven at 50ºC for 2 hours. ASTM D7137M-12 standard compression specimens of dimension150 mm long, 100 mm wide were then cut from the fabricated laminates using abrasive water jet cutting machine.

2.2 Repair Technique

To simulate damage on the fabricated compression specimen, a 30 mm diameter circular hole was produced at its geometrical center. This was achieved using a high precision water jet cutter. Subsequently, the damaged region was repaired by filling different adhesive reinforcements. Prior to repair procedure, the dressed specimens were polished using sand paper and further cleaned with acetone solution as per standard ASTM D2093 to remove the surface contaminations and debris so that better bonding interface can be achieved between the parent laminate and repair material. Since this study aims to examine the compressive restoration effects of various phases of adhesive reinforcements, the external patches were avoided and more interest was given to study the centrally filled adhesive reinforcements. Three different types of adhesive reinforcements (supplied by Marktech Composites, India) were considered in this study: (a) micro sized particulate glass fibres (average size 175–250 µm), (b) randomly oriented chopped glass fibres (nominal length of 4-6 mm), and(c) continuous unidirectional glass fibres (220 g/m^2) of stacking sequence $(0/90/90/0)_{2s}$. For the repairs with continuous fibres, care was taken to maintain accurate fibre orientation (i.e. $(0/90/90/0)_{2s}$) of the repair layup so as to ensure repair layup (i.e. orientation) is consistent or compatible with the parent laminate. Furthermore, this enable to investigate the influence of repairing the damaged area with a filler material similar to that of parent laminate in terms of material system and orientation. The dressed specimens were repaired using resin reinforced by particulates/fibres in a 1:1 ratio by weight. The surplus resin remaining on the adherent surface after repair was carefully removed using acetone solution. To investigate the efficiency of adhesive reinforced repair under compression loading, conventional neat epoxy filled repair specimens, notched specimens and virgin specimens were also fabricated. These specimens were used as the standard specimens for reference. Figure 1 shows the structure of the types of specimens considered in this study. Post-curing of all the fabricated specimens was performed at 50ºC for about 2 hours as they offer superior impregnation of the reinforcements and hence strong fibre-matrix bonding strength [34].

2.3   *Compression testing under digital image correlation and acoustic emission monitoring*

To evaluate the residual compression strength of repaired composite laminates, quasi-static compression tests was performed using an ASTM D7137M-12 anti-buckling compression fixture. A 100 kN maximum load capacity Tinus Olsen Universal Testing Machine (UTM) was employed to carry out the compression test. The crosshead speed of the machine was fixed at 0.5 mm/min. The compression tests were done at ambient environmental conditions. A total of five specimens were tested in each category and the averages of results were considered for interpretation. The online A.E. nondestructive technique was used to monitor the failure modes during different stages of compression loading. An Acoustic Emission setup integrated with 3 mega-samples per second (MSPS) sampling frequency SAMOS E3.10 data acquisition system and a 40 dB pre-amplifier was utilized to monitor damage progression in the specimens. The ambient noise signals were avoided from acquisition by setting the amplitude threshold at 45 dB. Two high precision wideband AE sensors of frequency range 100-900 kHz were used for damage monitoring. Specifications of AE sensor considered in this study are summarized in Table 4. During the compression test, the AE sensors were coupled above the specimen surface with the aid of silicon grease. The AE sensors were located 100 mm ahead of each other at diametrically opposite position around the repair area on the glass/epoxy specimens. The AE sensors were mounted on the rear side of the specimen to enable DIC monitoring on the front side. To determine the wave velocity of the glass/epoxy specimens, ASTM E976-10 pencil break test was conducted. The average wave velocity was found to be 3146.3 m/s. DIC images were recorded using a Nikon 5300 24.2 megapixel DSLR camera (see Figure 2(a)) with a frame rate of 29.97 frames per second (fps) for the entire period of the test. The camera was placed on a tripod stand having integral spirit level to make sure horizontal level. The specimens were placed by mechanical grips and care was taken concerning the alignment of the specimen. The camera was also accurately aligned relating to the mounted specimens. The lens was adjusted to attain better view and further to pass up pixels saturation over the view. Afterwards, the camera was calibrated for its location and alignment employing a suitable calibration grid plate. Camera was linked to workstation computers and the images are acquired at a predefined rate. An80 × 60 mm^2 region of interest (ROI) was employed. Region of interest was fixed or zeroed on by altering the focal length of the camera lens. To track the deformation of the laminate, a speckle pattern was applied over the front side of the glass/epoxy. Surface of test specimen was applied with target pattern (see Figure 2(b)). This was achieved by paint speckle using paint spray-can containing a nozzle of diameter 0.5 mm. This process was done by completely spraying white paint over the surface of the specimens and then partially spraying matte black colors with a paint spray-can. The droplet average dimension formed from the nozzle applying at a distance of around 500 mm from the test specimen was in the range of size 220–440 mm. Pixel subset size of 64×64 was selected for the DIC analysis. This size guaranteed that speckle pattern were sampled by as a minimum of 3×3 pixel array and every pixel subset included at least nine speckles as a result minimizing the chance of peak locking. Figure 2 (b) illustrates the subset dimension (0.256mm). The full field median longitudinal strains were mapped using Ncorr

software. On post-processing, the DIC images were extracted from the captured video at a rate of 5 fps. The DIC procedure was done as per the procedure highlighted in [35]. Figure 3 shows the workflow followed in this paper.

3. Results and discussion

3.1 Observations of surface damage

The main step in evaluating the structural performance of a repaired composite specimen is to characterize the damage pattern developed in the fractured specimens. Figure 4 (a-f) depicts the photographic image of the damage pattern for virgin and different repaired glass/epoxy specimens. In-plane compression tests on virgin specimens showed local buckling (i.e. critical fibre micro-buckling) surrounding the geometrical center of the specimen with associated resin cracking and fibre matrix debonding at the edges (see Figure 4 (a)). In the same condition, damaged specimens exhibited critical fibre micro-buckling at the transverse boundary of the hole perpendicular to the loading direction (see Figure 4 (b)). It was evident from the photographic images that the specimens repaired with neat epoxy (see Figure 4 (c)) and continuous fibres (see Figure 4 (f)) presented a damage pattern in the parent laminate similar to the damaged specimens because the crack propagated completely around the repair boundary (i.e. parent-repair material interface) and further progressed through micro-buckling of the fibres from the edge of the repair periphery perpendicular to the loading direction. No sign of damage was noticed at center of the repair site for these specimens. This evidently indicates that the load was unevenly transferred over and around the damaged site and enhances the stress concentration around the periphery of repaired region. Conversely, the specimens repaired using particulate fibres (see Figure 4 (d)) and chopped fibres (see Figure 4 (e)) exhibited significant damage at the center, approaching the damage pattern of virgin laminates. This indicates that most of the load was evenly transferred over and around the repaired material, preventing a stress concentration around the damaged site. Minor crack density on the parent laminate further supports these results. The reasons for these observations were explained by correlating the mechanical test results, DIC trends and AE signatures of different glass/epoxy specimens under in-plane compression loading.

3.2 Mechanical testing results

Plots for specimens subjected to the quasi-static compression test are shown in Figure 5 and illustrate (a) load-displacement, (b) ultimate failure load and (c) in-plane stiffness. The ultimate compression load for undamaged virgin specimens was found to be 64.6 kN. The damage induced in the glass/epoxy specimen in the form of circular hole of diameter 30 mm reduces the ultimate compression load by 39.16 %, leading to a failure load of 39.3 kN. Therefore ultimate compressive failure loads for repaired systems were as expected to fall within this range. A comparison of the repaired systems in plots shown in Figures 5 (a) and (b) clearly indicates that the chopped fibre reinforced adhesive repair specimens exhibited the greatest retention of strength in contrast to the specimen repaired using convention neat epoxy resin.

Damaged glass/epoxy specimens repaired using different phases of adhesive reinforcements like micro sized particulate glass fibres, randomly oriented chopped glass fibres and continuous glass fibres improves the average residual compressive strength by 16.30 %, 18.91 % and 13.91 %, respectively, in comparison to the specimens conventionally repaired using neat epoxy resin. Compression behaviour of different repaired specimens is summed up in Table 5. As this paper investigates the effect of introducing different phases of fibre reinforcement in epoxy matrix at the dressed site in adhesively bonded external patch repair for damaged glass/epoxy composites, the compression response and damage mechanisms of the specimens repaired using different phases of adhesive reinforcements was compared with the specimens conventionally repaired using neat epoxy resin. To better understand the repair performance and damage mechanisms of different repaired specimens, the virgin and damaged specimens were also considered in this study. It is interesting to note that the ranking order of ultimate failure load and stiffness between the material systems correlate well, as shown in Figures 5 (b) and (c) respectively. It is therefore possible that the stiffness of the repair can influence the failure load as discussed later.

3.3   AE and DIC results

Detailed analysis of the AE cumulative counts behavior plays a significant role in illustrating the damage mechanisms and failure evolution of composite laminates. The profile of the AE cumulative counts curve significantly changes as the compression load increases. The investigation of AE cumulative counts of different composite laminates allows a sequential classification of distinct zones of damage during quasi-static compression loading. The sequential classification of distinct zones of damage using AE cumulative counts has previously been reported by Jefferson et al. [36]. They investigated the nature and extent of damage in multiple times impacted glass/epoxy laminates subjected to compression loading, using a correlation of passive image processing and online acoustic emission techniques. They showed that AE cumulative count curve exhibits three distinct damage zones for the considered laminates under quasi static compression test. The damage profile includes three stages:

I. AE cumulative counts initiates (Location 1) directly after the onset of first damage and the curve advances with a slope closely equal to zero up to damage progression (Location 2) [36].

II. A gradual variation in the slope of AE cumulative count curve. This moderate increment in the AE response is accentuated by the evolution of macroscopic damage modes (Location 2) like debonding of the fibre/matrix interface and minor fibre failure [36].

III. A steep increase in the slope of the cumulative curve (Location 3) can be observed until up to rupture (Location 4). During final stages of mechanical loading, the counts of the AE waveform were much higher, associated predominantly with fibre failure. This variation in the counts of AE hits was extensively reflected in the slope of the AE cumulative counts curve at ultimate failure. This subsequent accumulation of

different damage hits is emphasized by an exponential growth of cumulative counts [36]. The investigation of the damage profile in each stage can be an important decisive factor in several applications from modification in repair processes through to estimation of the extent of damage during service.

In Figure 6 and 7, four locations during the compression loading have been marked as 1, 2, 3 and 4. The four consecutive points were respectively attributed:

1. Damage initiation (First AE events or permanent damage detected)
2. Damage propagation (Occurrence of macroscopic failure)
3. Unstable damage growth (Ultimate load is reached)
4. Laminate failure (Rupture) [36].

The correlations between compression properties, AE behavior and DIC trends for virgin specimens are shown in Figures 6 (a) and 7 (a). Strain values at the marked locations in the cumulative counts–time curve were estimated by averaging full field longitudinal strain measurements in the loading direction. The first AE hit was detected at 57.1 kN. The slope of AE cumulative counts curve raises significantly after the initiation of stage II around 61.7 kN and grow steeper during the unstable damage growth process (Stage III) up to rupture. At locations marked as 1 (e_y = 1.4 % strain at 57.10 kN) and 2 (e_y = 1.5 % strain at 61.7 kN), uniform strain distribution was observed in the associated DIC images in Figure 7 (a), strongly indicating uniform transfer of load until up to initiation of stage II. The later AE behavior was associated with intense fibre micro buckling processes up to rupture of the specimen, as shown in Figure 4 (a). In the cumulative counts curve, stage III (e_y = 1.82 % strain at 64.6 kN) was well emphasized with an exponential form of fit. The corresponding median longitudinal strain at the end of stage III was 1.99 %. Median longitudinal strain presents a significant increase in their value exactly at location 3, with AE hits indicating a large rise in the cumulative counts, while considerably less cumulative counts was noticed past location 3. The DIC trends exactly support the AE behaviour, while the damage progression increases abruptly with load.

The correlations between compression properties, AE behaviour and DIC trends for damaged (notched) specimens are shown in Figures 6 (b) and 7 (b). The first AE hit occurred much earlier at 26.7 kN compared to virgin specimens. It is interesting to observe that although at this location the AE results depict damage initiation qualitatively, the full field DIC results evidently point out the formation of incipient damage and their corresponding strain on the specimen, as depicted in Figure 7 (b). At stage II, the AE cumulative counts was distinctly characterized by early onset of damage progression phase (stage II) at 31.6 kN. As expected, at location 2 (e_y = 0.99 % strain at 31.60 kN), the strain images started to depict ''localized concentrations'' at the transverse boundary of the hole perpendicular to loading direction. The DIC results depicted a significant rise in strain at location 3 (e_y = 1.20 % strain at 36.70 kN). In addition, critical damage propagation was also noticed (see Figure 4(b)). In cumulative counts curve, evolution from parabolic to exponential nature (Stage III) was noticed at a compression

load of 36.7 kN, while for virgin specimens, no AE hits or visible damage was detected. At location 4, the longitudinal strain ultimately increases with an impressive 1.36 % increase for a small increase in compression load of 39.36 kN. This poor load carrying capability and substantial variation in the AE behaviour was emphasized due to the critical strain zone evolution around the notched region even at the initial stages of loading (26.7 kN) as depicted in Figure 7 (b).

Figures 6 (c) and 7 (c) depict the effect of a conventional homogeneous neat epoxy repair under compression. As depicted in Figure 5 (b), the neat epoxy specimens shows poor load carrying capability among the repaired specimens. The variation in the compression response as well as in the AE signatures due to poor structural integrity of neat epoxy specimens was well reflected on the parent/repair material interface, as can be evidently noticed from the DIC results. Repairing the damaged laminate with adhesive material shifted the incipient damage zone and its corresponding strain value. Damage initiation (stage I) occurred around the periphery of repair material at the longitudinal edge parallel to loading direction. This damage process begins at about 29.8 kN (ey = 0.88 % strain at 29.8 kN), closely approaching that of damaged specimens. After 45.6 kN at stage III (ey = 1.45 % strain at 45.6 kN), primary crack growth saturated on the parent/repair material interface; primary cracks were observed initiating on the parent material and progressed towards the specimen edges (see Figure 4(c)). The progression of such cracks evidently indicates the development of a highly stressed concentration zone around the repair accompanied with non-uniform transfer of load in and around the repair material. At the end of stage III (ey = 1.57 % strain at 45.2 kN), the homogeneous neat epoxy repair material completely debonded from the parent laminate. Among different repaired specimens, the glass/epoxy specimens repaired with homogeneous neat epoxy repair material exhibited the lowest in-plane stiffness compared to the virgin specimens (see Figure 5 (c)). This stiffness mismatch between the repair and parent material has the potential to cause debonding between the parent-repair material interfaces due to a built up of stresses at this interface. The debonding consequently leads to a discontinuous strain profile shown in the DIC images. Since the repair was of a lower stiffness, the load carrying capability across this repair region was reduced; hence there is greater amount of stress towards the outer edges of the repair region (i.e. on the parent laminate). In the case of specimens repaired using neat epoxy resin, stages II and III was the dominant zone which featured large longitudinal strains and critical damage growth, which were suppressed by the adhesive reinforced repair.

Figures 6 (d) and 7 (d) show a correlation of compression, AE and DIC responses of particulate fibre reinforced adhesive repaired specimens, in terms of load-time curve, AE cumulative counts and median longitudinal strain. The effect of particulate fibre reinforced adhesive repair on the residual strength was easily noticed by the unique DIC and AE behaviors and hence distinct type of damage profile. In the case of the particulate fibre specimens, until up to 42.9 kN, no AE hits occurred and were moderately generated as the compression load increased beyond this load. The compression load for the onset of the first AE hit was

significantly higher for the particulate specimens compared to the conventionally repaired neat epoxy specimens. A promising method of estimating the improved structural behaviour of the repaired specimens is by measuring the median longitudinal strain and load corresponding to the onset of damage initiation (stage I) and damage propagation (stage II) stages. From Figure 6 (d) and 7 (d), the median longitudinal strain and load for the onset of stage I (ey = 1.18 % strain at 42.9 kN), and stage II (ey = 1.34 % strain at 48.5 kN) was significantly higher compared to that of neat epoxy specimens. Based on these results, it is suggested that the addition of particulate fibre to the resin matrix increases the stiffness of repair material closer to that of the parent laminate (Figure 5 (c) supports this result). The closer matching stiffness profile between the repair and parent material reduced the extent of premature debonding(see Figure 4 (d)) at the parent-repair material interface compared to specimens repaired with neat epoxy At initiation of stage III, around 52.8 kN, different damage profiles were observed (see Figure 7 (d)), where the interface debonding grows in a controlled manner symmetrically on both side of the repair material (in the loading direction) unlike neat epoxy specimens. The AE results show a change in time history of AE cumulative counts from gradual growth to exponential one at stage III around a load of 53.5 kN (stage III), which was an evident indication of occurrence of fibre related failure (i.e. fibre micro-buckling) [36]. The compression, AE and DIC results highlight that the interface debonding generated just prior to sufficient compression load attains a level for fibre micro buckling at 53.5 kN with high median longitudinal strain (location 4, ey = 1.69 % strain at 53.5 kN). Thus, the major fracture leading to ultimate failure of the specimens starts at the interface which append near the final loading stage (location 4) with a minor density of crack into the parent laminate.

Figures 6 (e) and 7 (e) shows a correlation of compression, AE and DIC responses of chopped fibre reinforced adhesive repaired specimens, in terms of load-time curve, AE cumulative counts and median longitudinal strain. At stage I, uniform strain mapping with some localized strain at the center of the specimen was detected. Among repaired specimens, the median longitudinal strain and its corresponding load for the onset of stage I (ey = 1.226 % strain at 48.5 kN), and Stage II (ey = 1.36 % strain at 50.8 kN) was significantly higher for chopped fibre specimens. Also, the stiffness of the glass/epoxy specimens repaired with chopped fibres closely approached that of parent laminates (see Figure 5 (c)). This better stiffness match between the repair and parent material may have restricted the premature debonding failure between parent and repair material interface and improved the load carrying capability compared to all other repair specimens. This mechanism was suppressed in the neat epoxy specimens and manifested in DIC results with fewer indication of interface debonding failure progression in the chopped fibre specimens. The great susceptibility against premature debonding of the interface may be responsible for partially localized strain distribution around the repair material at the beginning of stage III (location 3). Similar to virgin specimens, at locations 3, the maximum longitudinal strain was noticed in and around the center of the specimen. This evidently indicates that the most of the compression load was distributed evenly between the repair material and parent laminate. Unlike the neat epoxy specimens, uniform strain distribution up to location 3

restricts the debonding effect around the repair material. This consequently improves the repair performance. Figure 4 (e) depicts typical damage modes for chopped fibre specimens. This stiffness match (i.e. improvement in the interface properties) between parent and repair material was more emphasized in the specimens repaired using particulate fibres and predominantly in specimens repaired using chopped fibres, where interface failure took place at higher load as compared to other repaired specimens. Moreover, the damage profile of these specimens observed form the DIC results were also completely different (i.e. no discontinuous strain profile) compared to neat epoxy specimens.

Figure 6 (f) illustrates the compression and AE responses of continuous fibre specimens. Furthermore, in Figure 7 (f), the damage progression profile in terms of DIC is illustrated by the presentation of strain maps. The median longitudinal strain at the onset of stage I (ey = 1.10 % strain at 35.7 kN), stage II (ey = 1.28 % strain at 42.6 kN) and stage III (ey = 1.54 % strain at 51.7 kN) was nearly close to that of neat epoxy specimens. The macroscopic occurrence of damage growth in the parent laminate was detected at a load of 42.6 N, which was higher than the values recorded for neat epoxy specimens. However, in neat epoxy and continuous fibre specimens the typical damage micro-mechanisms occurred around the periphery of the repair material at location 2. Similar to the neat epoxy specimens, the continuous fibre reinforced repair specimens had a lower stiffness as compared to parent laminate (see Figure 5 (c)). The voids in the resin rich region at the parent repair material interface might have reduced overall stiffness of the specimens (see Figure 8). A crack initiating in the resin rich region may propagate to the boundary of the repair and cause a complete interface debonding due to following the path of least resistance. These features might be responsible for premature debonding and reduction of the integrity of continuous fibre reinforced repair specimen. In addition, for both neat epoxy and continuous fibre specimens, the dominant damage mechanism can be pointed out by critical micro-buckling of the fibres around the repair boundary (see Figures4 (c) and 4 (f)). Similarly, the median longitudinal strain to ultimate failure (i.e. at location 4) of the continuous fibre specimen was lower (ey = 1.66 % strain at 52.4 kN) when compared to other adhesive reinforced repair specimens, providing further evidence on the low energy fracture interfaces in continuous fibre specimens. The strain field and damage growth on continuous fibre specimens follows similar pattern as that of neat epoxy specimens. These investigations can be further confirmed by using damage mode distribution of different glass/epoxy specimens under quasi static compression tests, described in the following sections.

3.4   Damage Mode Investigation

k-means ++ clustering analysis was performed for discriminating AE data sets generated during quasi-static compression testing [37-38]. The application of pattern recognition approach for the characterization of AE signals has been proposed the past decade to overcome disadvantages of conventional clustering techniques using single AE parameters, such as peak frequency, amplitude, RMS values, etc. Most investigations have employed conventional AE parameters, such as amplitude, duration, counts, and energy, to classify between various AE

signals and their relationship to the onset of damage mechanisms [37-40]. None of the single parametric based approach explains in depth filtering procedure and in many cases the quality of AE signals and noise filtering mainly depends on experience of operator. Each AE signal can be allied with a pattern composed of multiple relevant descriptors. The concurrent study of different AE parameters makes it feasible to attain more reliable information for detection of AE source mechanisms, particularly when allied with pattern recognition algorithms. Pattern recognition techniques are used as a complementary and/or alternative AE signal processing tool, to the better established knowledge based systems, focusing to help users in identification of noise and/or filtering and assisting better discrimination of AE signals. Unsupervised k-means++ analysis of recorded AE events helps in clustering the damage modes generated in the virgin and different repaired specimens, with adequate accuracy [37-38]. The idea is essentially that each damage mode produces an AE event, which is associated in turn to the amplitude of strain energy dissipated as the effect of damage in the specimens. As a result, each AE event has unique characteristics, in the sense that its RMS value, amplitude, counts, duration, frequency and other signal features are related to the failure mechanisms, such as matrix or resin cracking, fibre/matrix debonding, and fibre breakage. The significance of this fact is that different clusters for AE events, associated respectively with matrix or resin cracking, fibre/matrix debonding and fibre breakage can be obtained. k-means++ analysis requires the optimum cluster number "k" and the high variance AE descriptors as input entries. To validate the number of clusters "k", the Davies–Bouldin (DB) and Silhouette coefficient (SC) cluster validity index has been evaluated [39-40]. The optimal number of distinct clusters should provide the least value of a DB index, which corresponds to better tightness of each cluster. Here, the most favorable value is likely to be less than one [39]. In contrast, Silhouette coefficient (SC) evaluates the similarities between different data within a cluster in comparison to data in another cluster. Here, the optimal number of distinct clusters should provide the highest value of Silhouette coefficient, indicating that a data is compatible to a particular cluster, and incompatible to the nearby clusters. In this case, the optimal value is expected to be in the range 0.6 to 0.7 according to [39].Figure 9 depicts the best possible number of clusters for virgin, damaged and different repaired glass/epoxy composite specimens. Based on these principles, in the above mentioned specimens, the higher limit for Silhouette coefficient and lower limit for Davies–Bouldin index coincides at cluster number three. Therefore, the multivariable k-means++ analysis was performed with three numbers of clusters for all the datasets and showed the optimum cluster quality. The AE parameters such as the amplitude, duration, energy, counts, rise-time, signal strength, absolute energy and the RMS value were used as a descriptor to perform the analysis [39-40]. The cluster validity evaluations for different specimens are summarized in Table 6. To visualize the relationships between different multidimensional AE parameters in a two-dimension subspace, k-means++ analysis was accompanied with Principal Component Analysis (PCA).

PCA is a quantitatively accurate method that aids the visualization of multiple AE variables, monitoring the damage progression of the composite specimens by replacing original variables with an orthogonal non-redundant new set of variables (principal components) in a

different coordinate system [41]. Figure 10 shows the cumulative sum of the variance and percentage variance of each principal component. The PCA representation depicts that all the points within each set of clusters were well concentrated. It was evident that the cumulative sum of variance of principal component of amplitude and duration AE parameters exceeds two third of the total variance. Since the AE parameters such as amplitude and duration of AE waveform were sufficient to evaluate the failure mechanisms that govern the damage progression of the glass/epoxy composite specimens, the data visualization was restricted to the first two principal components. Figure 10 depicts the PCA projection of the three types of clusters (nominated as T1, T2 and T3) of AE hits to two-dimensional sub space by principal components of amplitude and duration parameters for virgin, damaged and different repaired glass/epoxy specimens. It was clear that AE hits were well discriminated by first two principal components.

Figure 11 illustrates that the distribution of the three clusters (Ty1, Ty2 and Ty3) for virgin, damaged and the four repaired glass/epoxy specimens were closely identical. Ty1 (45 – 56 dB) have short duration, Ty2 (56 – 72 dB) have slightly higher amplitude compared to Ty1 and AE hits in Ty3 (69 - 100 dB) have higher amplitude ranges compared to other clusters. These distinct ranges can perhaps be related with different failure mechanisms. Many literatures can be found on acoustic emission amplitude-based discrimination. In the literature, Arumugam et al [42 and 43] have also reported three major damage modes to depict damage process in glass/epoxy composite laminates which are similar to the attributes of amplitude ranges described here. Arumugam et al [42] have investigated the amplitude distribution of AE waveform from tensile tests on GFRP composite laminates. They reported that the AE signals with low to medium amplitude are allied with matrix or resin cracking, those with moderate amplitude ranges allied with interface debonding and lastly, those with medium to high amplitude allied with fibre breakage. Kotsikos [28] associated a few ranges of amplitude to various damage mechanisms identified in glass/epoxy composites under fatigue load. He ascribed the low amplitude range (from 40 to 55 dB) to the resin or matrix cracking, then from 55 to about 70 dB (i.e. moderate amplitude ranges) to the interface debonding failure and lastly, beyond 70 dB to the fibre failure. The work of Li [41] and Barre and Benzeggagh [29] also shows similar behavior of the amplitude ranges for GFRP laminates. Most of the authors tell contradictory amplitude ranges for various damage modes. However, it is frequently reported and well accepted in most of the literature that the AE signals with least amplitude ranges correspond to matrix or resin cracking, those with highest amplitude ranges correspond to fibre failure, and those with mid-amplitude ranges relate to delamination or fibre/matrix debonding damage modes [27-29, 42-43]. Therefore, the pertinent amplitude ranges were: 45 – 56 dB related to the matrix or resin cracking, 56 – 72 dB to the fibre/matrix debonding and 69 - 100 dB to fibre micro-buckling, respectively. Figure 12 shows close up photographs of different failure modes in the glass/epoxy specimens.

Signals in Ty1 and Ty2 were significantly overlapped at the boundaries of the clusters, and cluster Ty2 was overlapped to some extent with the Ty3 cluster (see Figure 11). To better

depict the density and similarities of AE hits discriminated under each clusters, the normalized number of AE hits versus cluster number plot for all the specimens are illustrated in Figure 13. All the glass/epoxy specimens have a maximum number of AE hits recorded under cluster Ty 1 (matrix cracking damage mode). For neat epoxy specimens, the occurrence of matrix cracking and debonding damage modes approaches those of the damaged(notched) specimens. Among the repaired glass/epoxy specimens, the chopped fibre specimens generated the least number of AE hits under all the three clusters numbers (Ty 1, Ty 2 and Ty 3). In addition to this, chopped fibre specimens have the maximum compression strength, observed in Figures 5 (a), 6 (e) and 7 (e). Figure 13 shows that the compression response of all the repaired specimens was largely governed by magnitude of the matrix cracking and debonding damage mode generated at the parent/repair material interface. AE results depict that the variation of the normalized number of hits in the Ty3 cluster (related to fibre micro-buckling) was insignificant for all the specimens. These characteristics clearly illustrates that the AE signals pertaining to the amplitude range between range 69 – 100 dB were immaterial with modification in the repair material. The enhanced performance of particulate fibre, chopped fibre and continuous fibre specimens can be evidently noticed by much less generation of AE hits pertaining to cluster Ty1 and Ty2. This might be due to the reinforcing fibre in the resin matrix reducing the AE hits pertaining to the matrix cracking and parent-repair material interface debonding. Reinforcing chopped fibre in the epoxy matrix made this reduction even more significant. The poor interface bonding strength in neat epoxy specimens induces the accumulation of Ty1 and Ty2 AE hits more significantly.

4. Conclusions

The role of various phases of adhesive reinforcements used to repair damaged glass/epoxy composite laminates subjected to compression loading was studied. The experimental results acquired from the compression test and detailed AE and DIC monitoring indicate the following conclusions:

1. The chopped fibre reinforced adhesive repair specimens exhibited the greatest retention of compressive strength, a ~19 % improvement compared to the neat unfilled epoxy resin. Between the particulate, chopped and continuous fibre adhesive repairs, there was <5 % difference to residual compressive strength.

2. The AE and DIC damage profile of the adhesive reinforced repair specimen differed to the specimen repaired conventionally using neat epoxy. This was emphasized by different AE behaviour and DIC trends in terms of cumulative counts and maximum longitudinal strain to failure respectively.

3. The stiffness match between parent and repair material was more emphasized in the specimens repaired using particulate fibres and predominantly in specimens repaired using chopped fibres, where interface failure took place at higher load as compared to other repaired specimens. Moreover, the damage profile of these specimens observed

form the DIC results were also completely different (i.e. no discontinuous strain profile) compared to other repaired specimens.

4. K-means ++ clustering analysis accompanied with Principal Component Analysis (PCA) was performed for discriminating AE data sets generated during quasi-static compression testing. Three distinct clusters (nominated as T1, T2 and T3) of AE hitswere disseminated ranging from low, medium and high respectively. Based on literature results, Ty 1, Ty 2 and Ty 3 AE hits were related to matrix or resin cracking, fibre/matrix debonding and fibre micro bucklingrespectively. The AE results signify thatreinforcing fibre in the epoxy matrix at the damaged site, led to a lower amount of matrix cracking and parent-repair material interface debonding damage compared to the neat resin ones. This was evidenced by a lower number of AE hits across the amplitude ranges.

References

[1] Richardson M W, Wisheart M J. Review of low-velocity impact properties of composite materials. Compos Part A – ApplSciManuf 1996; 27A:1123–31.

[2] Cantwell W J, Morton J. The significance of damage and defects and their detection in composite materials: a review. The Journal of Strain Analysis for Engineering Design1992; 27(1):29–42.

[3] Caprino G. Residual strength prediction of impacted CFRP laminates. J Compos Mater 1984; 18:508–18.

[4] Mahendra Thunga, Wilber Y. Lio, Mufit Akinc, Michael R. Kessler. Adhesive repair of bismaleimide/carbon fibre composites with bisphenol E cyanate ester Composites Science and Technology 2011;71: 239–245.

[5] Cheng P, Gong XJ, Hearn D, Aivazzadeh S. Tensile behaviour of patch-repaired CFRP laminates. Compos Struct 2011; 93:582–9.

[6] Katnam K B, Da Silva L F M,Young T M. Bonded repair of composite aircraft structures: A review of scientific challenges and opportunities a Progress in Aerospace Sciences 2013; 61: 26–42.

[7] Everett A. Westerman, Jr. inventors; Method for repairing a hole in a structural wall of composite material. US 4978404 A. 1990 Dec 18.

[8] Rider A N, Wang C H, Chang P. Bonded repairs for carbon/BMI composite at high operating temperatures. Composites: Part A 2010; 41: 902–912.

[9] Campilho R D S G, Moura M F S F, Modelling J J M S. Modelling single and double-lap repairs on composites materials. Compos SciTechnol 2005; 65:1948–58.

[10] Mohammad Kashfuddoja, Ramji M. Design of optimum patch shape and size for bonded repair on damaged Carbon fibre reinforced polymer panels. Materials and Design 2014; 54: 174–183.

[11] Liu X, Wang G. Progressive failure analysis of bonded composite repairs. Compos Struct 2007; 81:331–40.

[12] Soutis C, Duan DM, Goutas P. Compressive behaviour of CFRP laminates repaired with adhesively bonded external patches. Compos Struct 1999;45:289–301.

[13] Khalili S M R, Shokuhfar A, Hoseini S D, Bidkhori M, Khalili S, Mittal R K. Experimental study of the influence of adhesive reinforcement in lap joints for composite structures subjected to mechanical loads. International Journal of Adhesion & Adhesives 2008; 28: 436– 444.

[14] Bakuckas John G, Westerman Bud. Fatigue and residual strength performance of bonded repair to metallic fuselage. Struct Integrity: Influence of Efficiency and Green Imperatives 2011; 8(2011):735–52.

[15] Sanchez-Saez S, Barbero E, Zaera R, Navarro C. Compression after impact of thin composite laminates. Compos SciTechnol 2005; 65:1911–9.

[16] Andrew TR, Richard B, Giles WH. Post-buckled propagation model for compressive fatigue of impact damaged laminates. Int J Solids Struct 2008; 45:4349–61.

[17] J. Andrew, V. Arumugam, A.P. Sidharth and B. Thomas. Acoustic Emission based Monitoring of Cut-out Geometry Effects in Carbon/Epoxy Laminates under Uni-axial Compression, Int. J. Vehicle Structures & Systems, 6(2014), 17-23.

[18] Jefferson Andrew, C. Ramesh. Residual Strength and Damage Characterization of Unidirectional Glass–Basalt Hybrid/Epoxy CAI Laminates. Arabian Journal for Science and Engineering 2015; 2191-4281.

[19] Bohse J. Acoustic emission characteristics of micro-failure processes in polymer blends and composites. Compos SciTechnol 2000; 60(8):1213–26.

[20] Wevers, M 1997, 'Listening to the sound of materials: Acoustic Emission for the analysis of material behaviour', NDT&E International, vol. 30, no. 2, pp. 99-106.

[21] Ni QQ, Kurashiki K, Iwamoto M, AE technique for identification of micro failure Modes in CFRP composites. Mater Sci Res Int 2001;7(1):67–71.

[22] Groot PJ, Wijnen PA, Jansen BF. Real time frequency determination of acoustic emission for different fracture mechanisms in carbon/ epoxy composites. Comp Sci Tech 1995;55(4):405–12.

[23] Woo SC, Choi NS. Analysis of dominant frequencies of glass–fibre/ aluminum laminates during acoustic emission measurement. Key Eng Mat 2006;321–323:901–6.

[24] J. M. Berthelo, J. Rhazi, Acoustic emission in carbon fibre composites, Composites Science and Technology 37 (1990) 411–428.

[25] Wadim JR. Acoustic emission applications. San Juan Capistrano, CA: Dunegan Enevco; 1978.

[26] Gong XL, Laksimi A, Benzeghagh ML. Nouvelle approche de l'émission acoustique et son application à l'identification des mécanismes d'endommagement dans les matériaux composites. Revue des composites et des matériaux avancés 1998;8(1):179–205.

[27] Kim ST, Lee YT. Characteristics of damage and fracture process of carbon fibre reinforced plastic under loading-unloading test by using AE method. Mater Sci Eng 1997; 234–236(A):322–6.

[28] Kotsikos G, Evans JT, Gibson AG, Hale J. Use of acoustic emission to characterize corrosion fatigue damage accumulation in glass fibre reinforced polyester laminates. Polym Compos 1999;20(5):689–96.

[29] Barre S, Benzeggagh M. On the use of acoustic emission to investigate damage mechanisms in glass-fibre-reinforced polypropylene. Compos Sci Technol 1994;52:369–76.

[30] Lopez-Anido R, El-Chiti F W, Muszyn˜ski L, Dagher H J,Thompson L D, Hess P E. Composite material testing using a 3-D digital image correlation system, COMPOSITES 2004 convention and trade show American composites manufacturers association. Florida,USA: Tampa; 2004.

[31] Sutton M A, Orteu J J,Schreier H. Image correlation for deformation and shape measurements. New York: Springer; 2009.

[32] Jefferson Cuadra, Prashanth A. Vanniamparambil, Kavan Hazeli, Ivan Bartoli, Antonios Kontsos. Damage quantification in polymer composites using a hybrid NDT approach. Composites Science and Technology 83 (2013) 11–21.

[33] J. Jefferson Andrew, V. Arumugam, K. Saravanakumar, H.N. Dhakal, C. Santulli. Compression after impact strength of repaired GFRP composite laminates under repeated impact loading. Composite Structures 2015; 133: 911–920.

[34] Jefferson Andrew J, V. Arumugam, C. Santulli. Effect of post-cure temperature and different reinforcements in adhesive bonded repair for damaged glass/epoxy composites under multiple quasi- static indentation loading. Composite Structures (2015), doi: http://dx.doi.org/10.1016/j.compstruct.2015.10.037.

[35] A.J. Comer, K. B. Katnam, W. F. Stanley, T. M. Young. Characterising the behaviour of composite single lap bonded joints using digital image correlation International Journal of Adhesion & Adhesives 40 (2013) 215–223.

[36] Jefferson Andrew J, Arumugam V,C. Santulli, Anitha Jennifers, Poorani M, 'Acoustic Emission Characterization of Failure Modes in Composite Laminates Subjected to Multiple Impacts using Digital Image Correlation, Journal of engineering technology, vol. 6, 2015.

[37] Arthur D, Vassilvitskii S. K-means++: the advantages of careful seeding. In: Proceedings of the eighteenth annual ACM-SIAM symposium on discrete algorithms: Society for Industrial and Applied Mathematics; 2007. p. 1027–35.

[38] A. Mareca, J. H. Thomasa, R. El Guerjoumaa. Damage characterization of polymer-based composite materials: Multivariable analysis and wavelet transform for clustering acoustic emission data Mechanical Systems and Signal Processing 2008; 22: 1441–1464.

[39] Li Li, Stepan V. Lomov, Xiong Yan, ValterCarvelli. Cluster analysis of acoustic emission signals for 2D and 3D woven glass/epoxy composites. Composite Structures 2014; 116: 286–299.

[40] R. Gutkin, C.J.Green, S.Vangrattanachai, S.T.Pinho, P.Robinson, P.T.Curtis. On acoustic emission for failure investigation in CFRP: Pattern recognition and peak frequency analyses. Mechanical Systems and Signal Processing 2011; 25: 1393–1407.

[41] Jolliffe I. Principal component analysis. Wiley Online Library; 2005.

[42] V. Arumugam, S. Barath Kumar, C. Santulli, S.A. Joseph. Effect of fibre orientation in uni-directional glass epoxy laminate using acoustic emission monitoring. Acta Metallurgica Sinica (English Letters) 2011; 24: 351–364.

[43] R.Asokan, M. Dinesh, V. Arumugam and R. Dhanaraj. Experimental Investigation of GFRP Lap Joint Failure Mechanisms using Acoustic Emission, Int. J. Vehicle Structures & Systems 2012; 4(2): 48-52.

[44] S.E. Mechraoui, A. Laksimi, S. Benmedakhene. Realiability of damage mechanism localization by acoustic emission on glass/epoxy composite material plate, Composite Structures, 94:1483-1494.
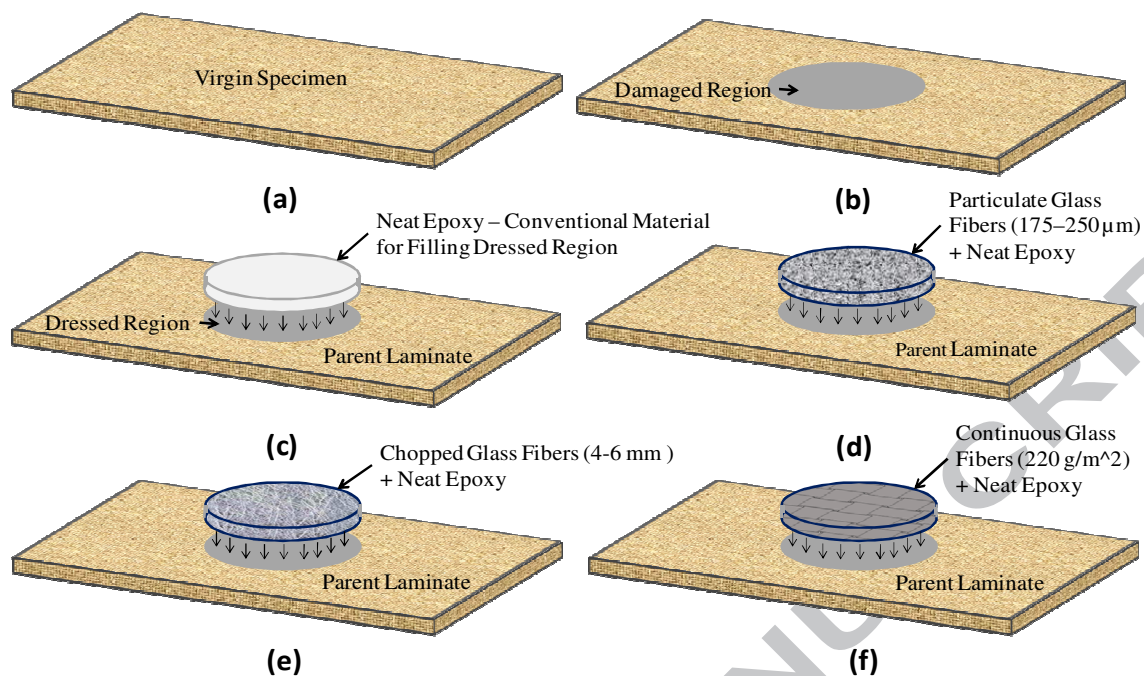
Figure captions:

Figure 1: Structure of different types of compression specimens (a) Virgin specimen (b) Specimen with circular notch, Specimens repaired using (c) Neat epoxy, (d) Particulate glass fiber (e) Chopped glass fiber and (f) Continuous glass fiber.
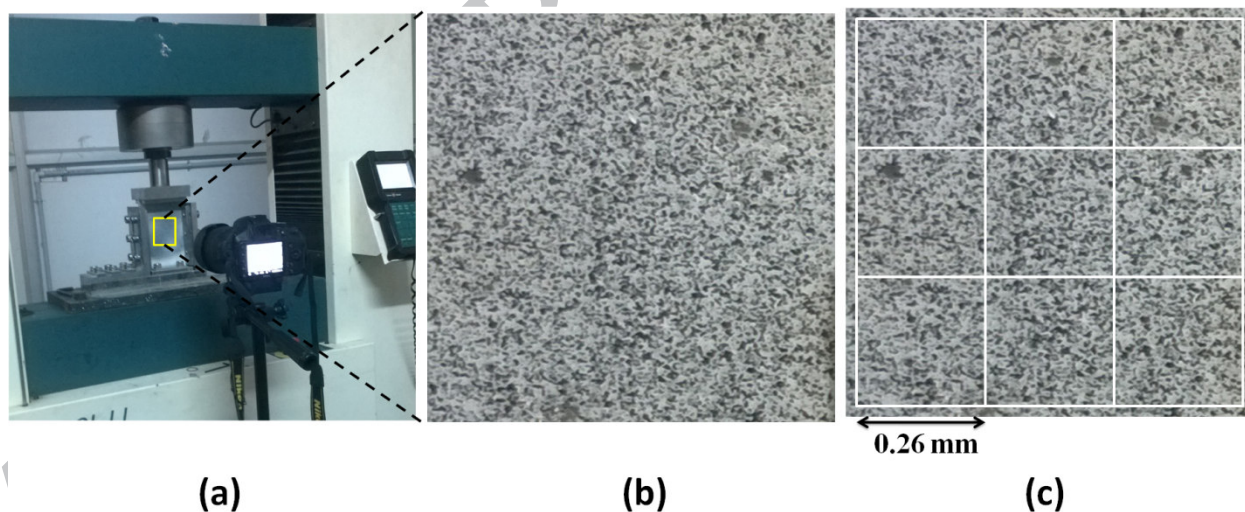
Figure 2: (a) Specimen under Static Compression Test, (b) Surface speckle and image texture and (c) 64×64 pixel subset size for the high magnification DIC test.
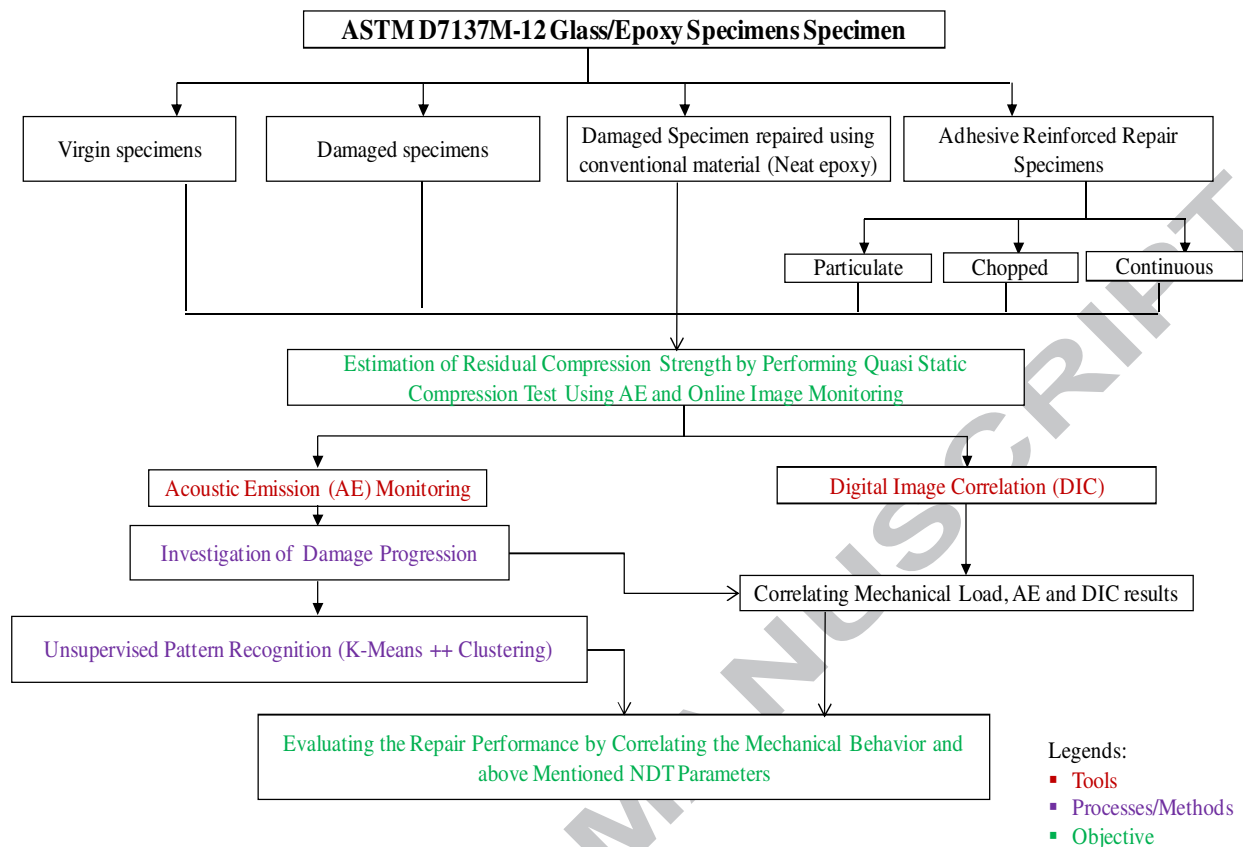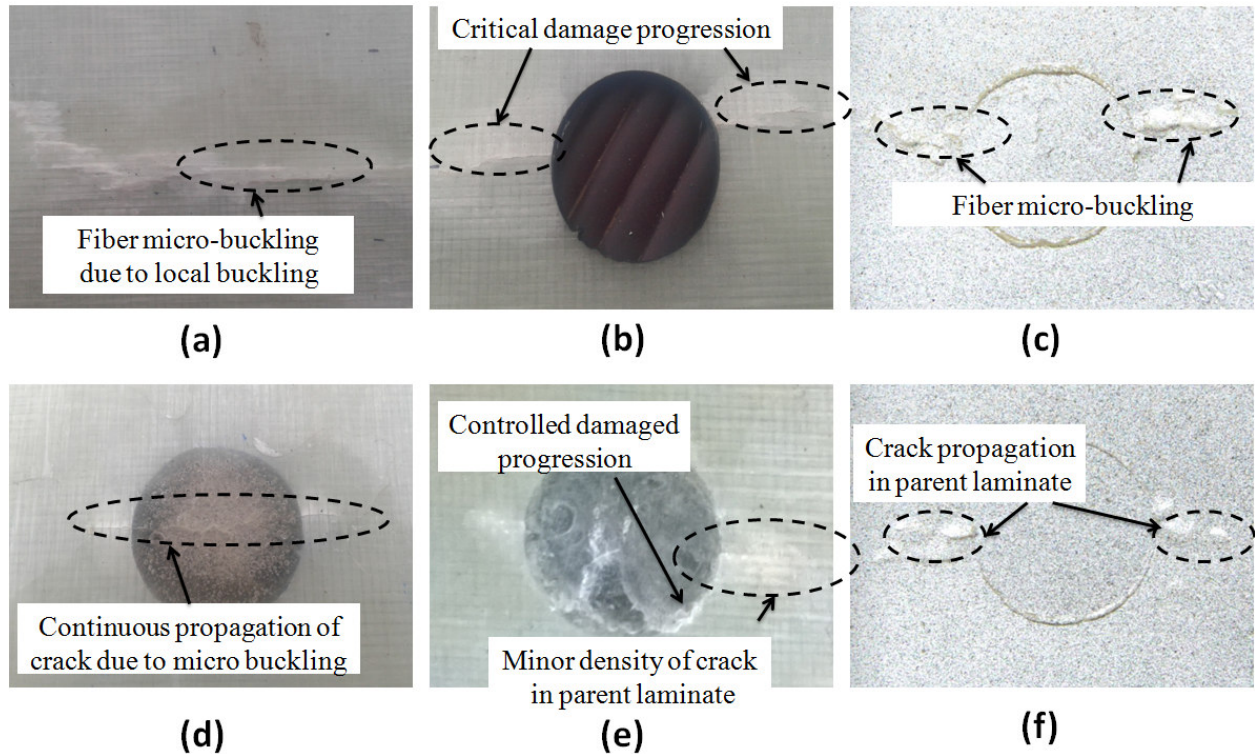
Figure 3: Workflow of this paper.

Figure 4: Photographic images of fractured specimens: (a) Virgin specimen (b) Specimen with circular notch, specimens repaired using (c) Neat epoxy, (d) Particulate glass fiber (e) Chopped glass fiber and (f) Continuous glass fiber.
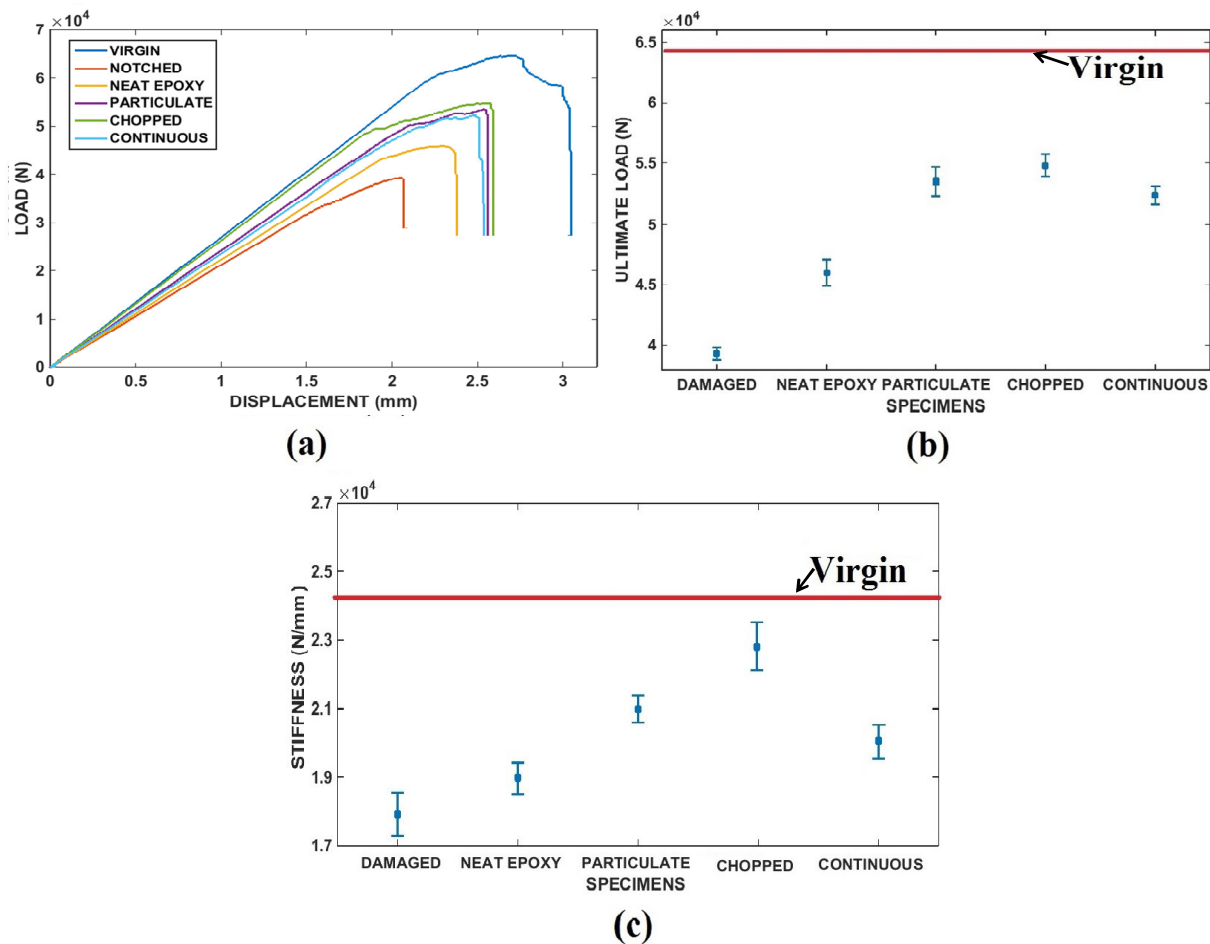
Figure 5: Quasi static Compression test results of virgin, damaged (notched) and different repaired glass/epoxy specimens: (a) Load vs. Displacement curves, (b) Ultimate load and (c) In-plane stiffness.
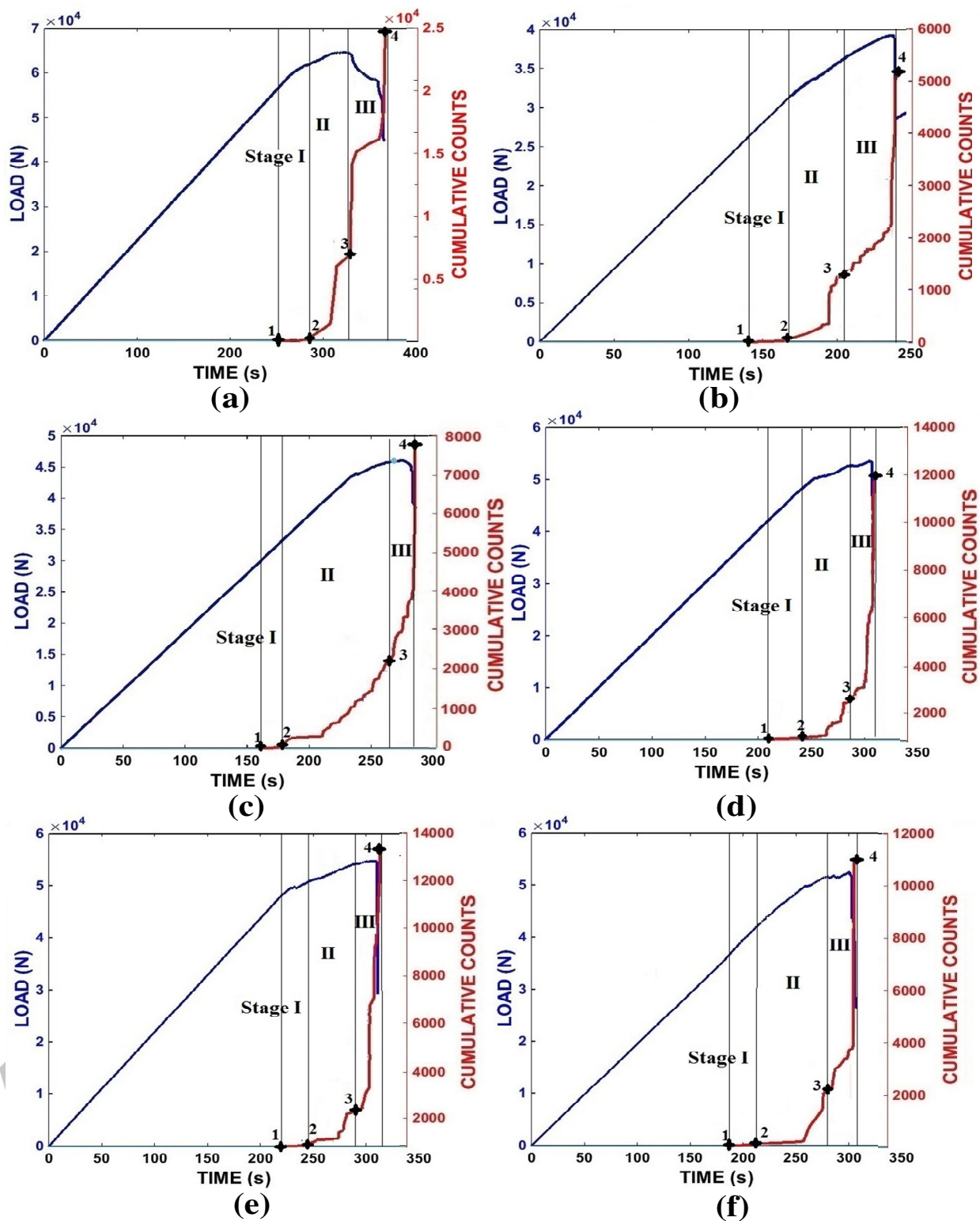
Figure 6: Compression response and AE behaviour of (a) Virgin specimen (b) Specimen with circular notch, Specimen repaired using (c) Neat epoxy, (d) Particulate glass fiber (e) Chopped glass fiber and (f) Continuous glass fiber.

Figure 7: Median longitudinal strain of (a) Virgin specimen (b) Specimen with circular notch, Specimen repaired using (c) Neat epoxy, (d) Particulate glass fiber (e) Chopped glass fiber and (f) Continuous glass fiber.

Figure 8: Photograph of specimen repaired using continuous glass fiber.

Figure 9: Davies–Bouldin index and Silhouette coefficient of (a) Virgin specimen (b) Specimen with circular notch, Specimens repaired using (c) Neat epoxy, (d) Particulate glass fiber (e) Chopped glass fiber and (f) Continuous glass fiber.

Figure 10: The variance of principal components and PCA visualization of k-means++ clustering of (a) Virgin specimen (b) Specimen with circular notch, Specimens repaired using (c) Neat epoxy, (d) Particulate glass fiber (e) Chopped glass fiber and (f) Continuous glass fiber.
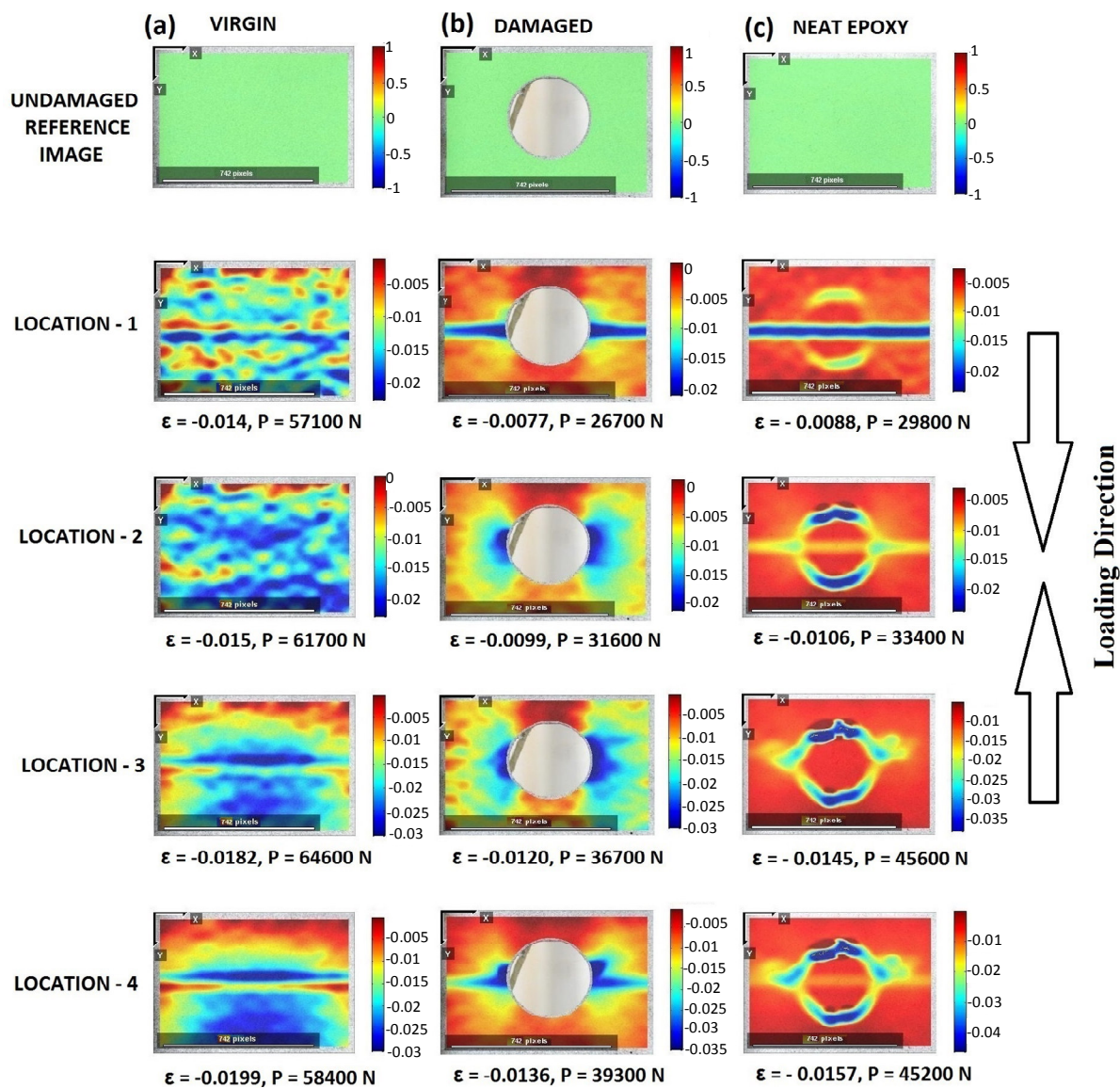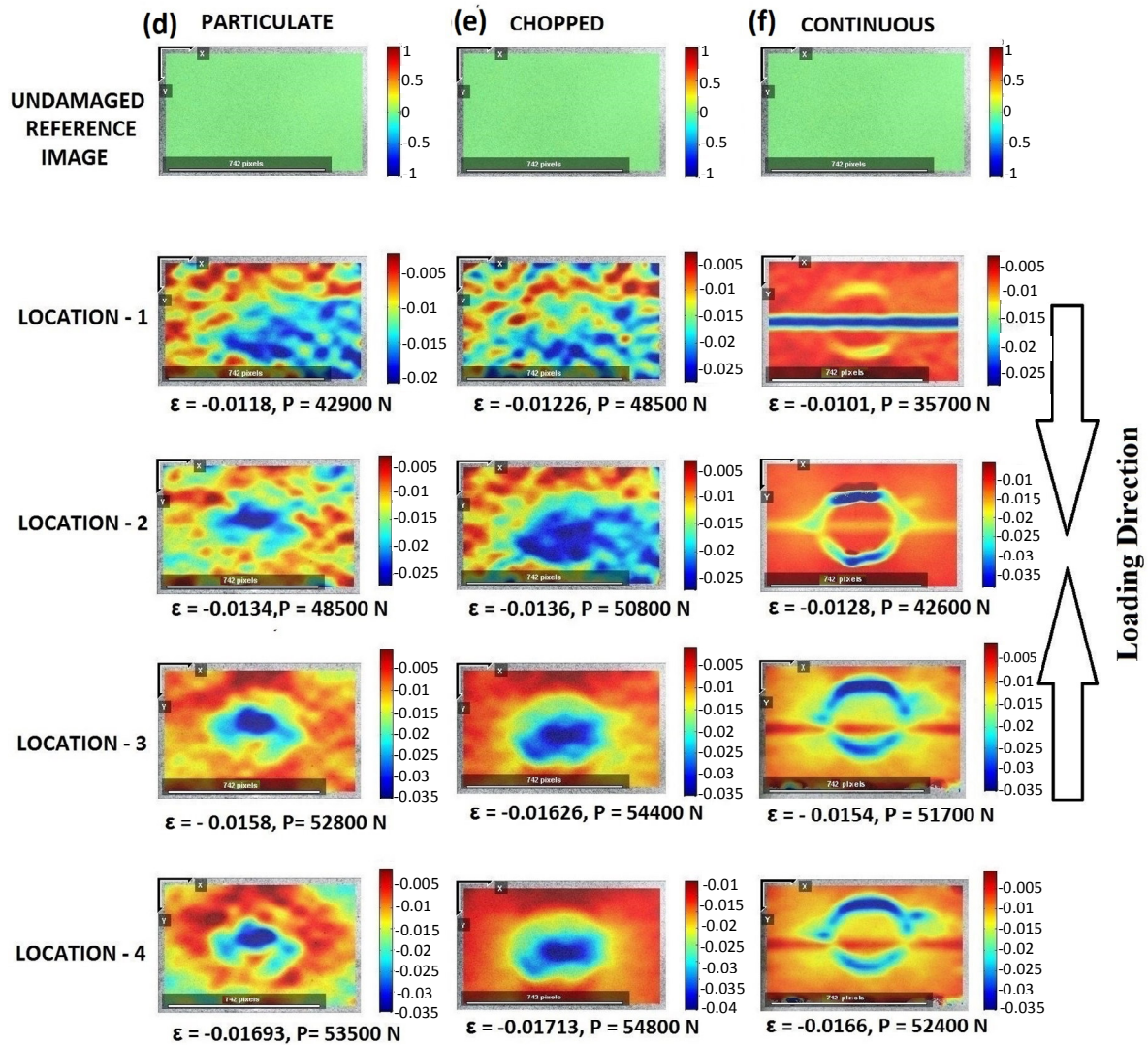
Figure 11: Cluster results discriminated by amplitude and duration for (a) Virgin specimen (b) Specimen with circular notch, specimens repaired using (c) Neat epoxy, (d) Particulate glass fiber (e) Chopped glass fiber and (f) Continuous glass fiber.

Figure 12: Close up photographs of different failure modes in the glass/epoxy specimens.

Figure 13: Normalized number of AE hits versus clusters of virgin, damaged (notched) and different repaired glass/epoxy specimens.

Figure 1: Structure of different types of compression specimens (a) Virgin specimen (b) Specimen with circular notch, Specimens repaired using (c) Neat epoxy, (d) Particulate glass fiber (e) Chopped glass fiber and (f) Continuous glass fiber.
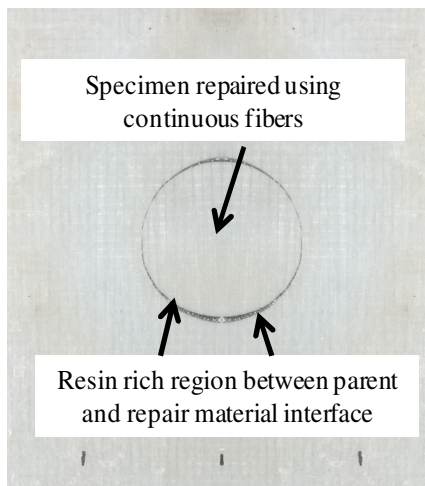

Figure 2: (a) Specimen under Static Compression Test, (b) Surface speckle and image texture and (c) 64×64 pixel subset size for the high magnification DIC test.

Figure 3: Workflow of this paper.

Figure 4: Photographic images of fractured specimens: (a) Virgin specimen (b) Specimen with circular notch, Specimens repaired using (c) Neat epoxy, (d) Particulate glass fiber (e) Chopped glass fiber and (f) Continuous glass fiber.
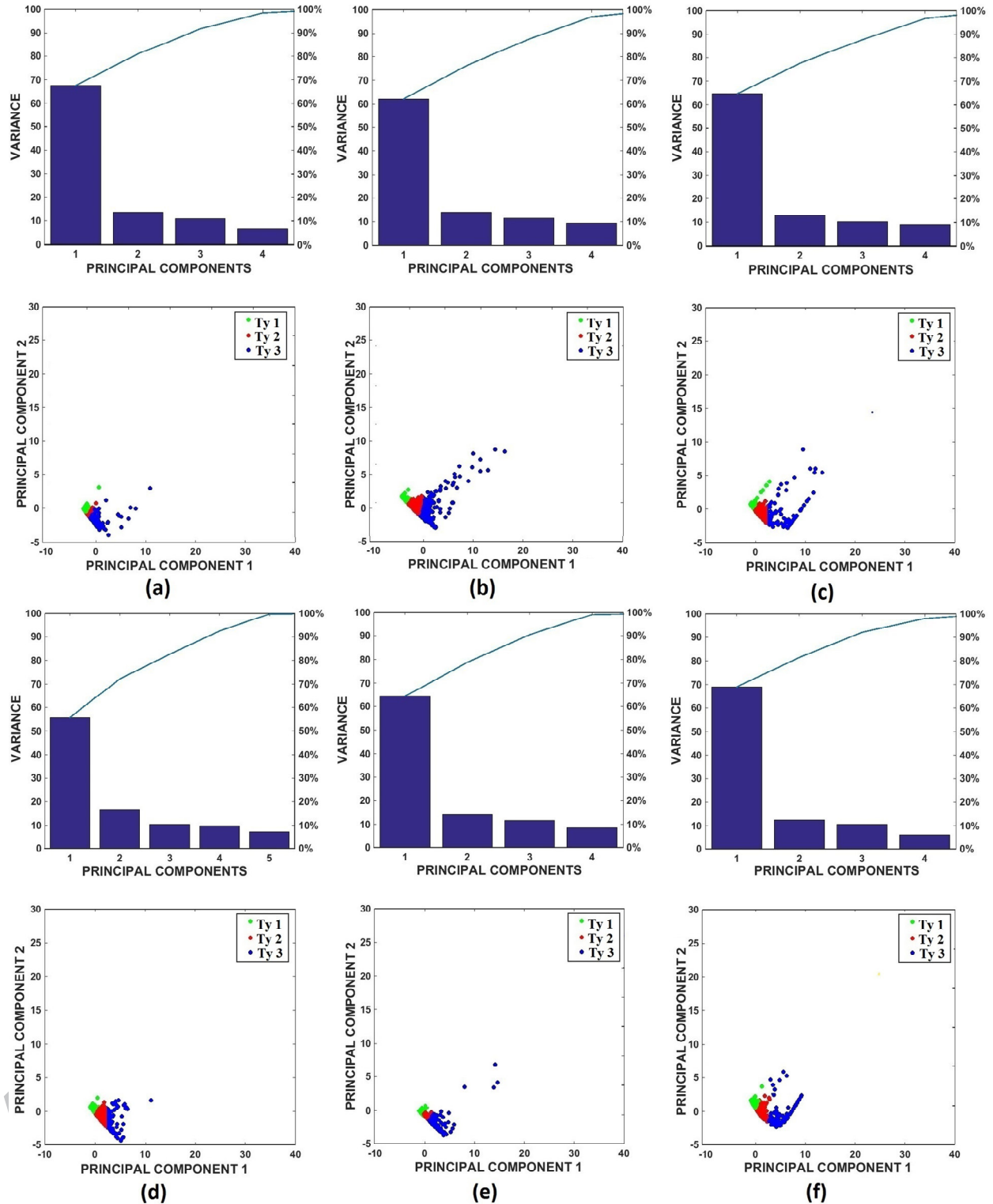
Figure 5: Quasi static Compression test results of virgin, damaged (notched) and different repaired glass/epoxy specimens: (a) Load vs. Displacement curves, (b) Ultimate load and (c) In-plane stiffness.

Figure 6: Compression response and AE behaviour of (a) virgin specimen (b) Specimen with circular notch, specimen repaired using (c) Neat epoxy, (d) Particulate glass fiber (e) Chopped glass fiber and (f) Continuous glass fiber.

Figure 7: (Continued).

Figure 7: Median longitudinal strain of (a) virgin specimen (b) Specimen with circular notch, Specimen repaired using (c) Neat epoxy, (d) Particulate glass fiber (e) Chopped glass fiber and (f) Continuous glass fiber.
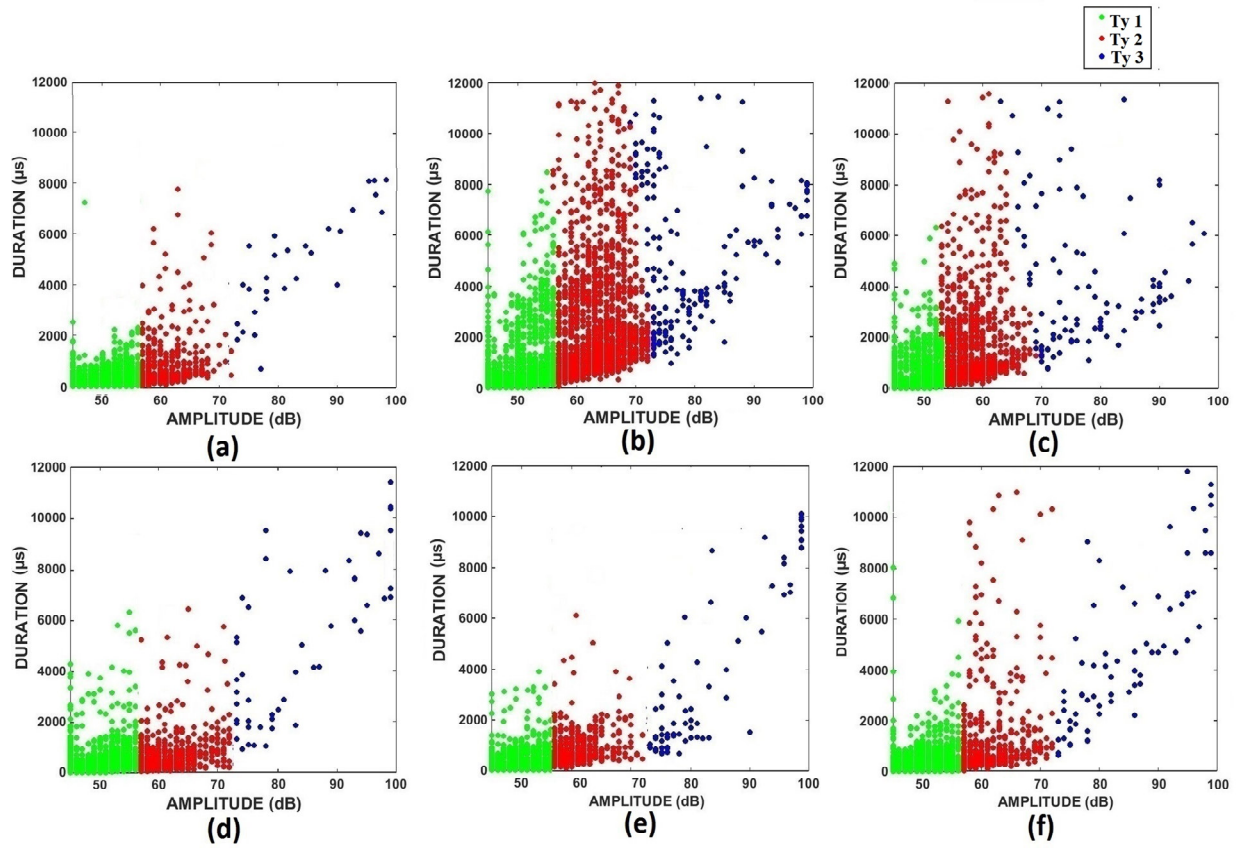
Figure 8: Photograph of specimen repaired using continuous glass fiber.

Figure 9: Davies–Bouldin index and Silhouette coefficient of (a) Virgin specimen (b) Specimen with circular notch, Specimens repaired using (c) Neat epoxy, (d) Particulate glass fiber (e) Chopped glass fiber and (f) Continuous glass fiber.
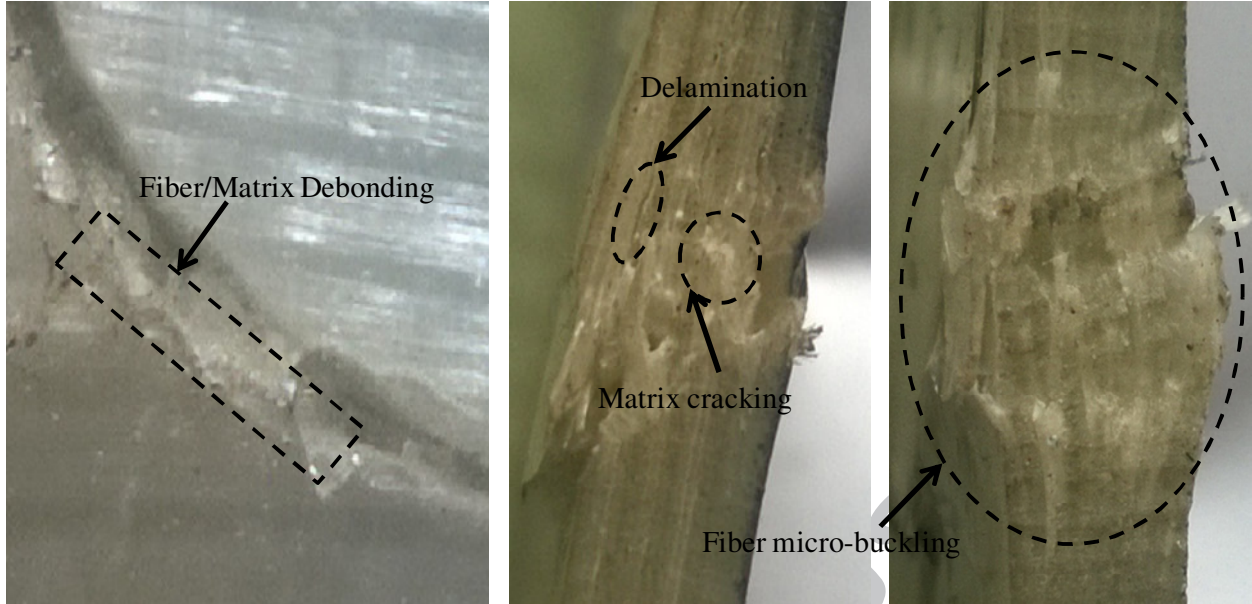
Figure 10: The variance of principal components and PCA visualization of *k*-means++ clustering of (a) Virgin specimen (b) Specimen with circular notch, specimens repaired using (c) Neat epoxy, (d) Particulate glass fiber (e) Chopped glass fiber and (f) Continuous glass fiber.

Figure 11: Cluster results discriminated by amplitude and duration for (a) Virgin specimen (b) Specimen with circular notch, Specimens repaired using (c) Neat epoxy, (d) Particulate glass fiber (e) Chopped glass fiber and (f) Continuous glass fiber.

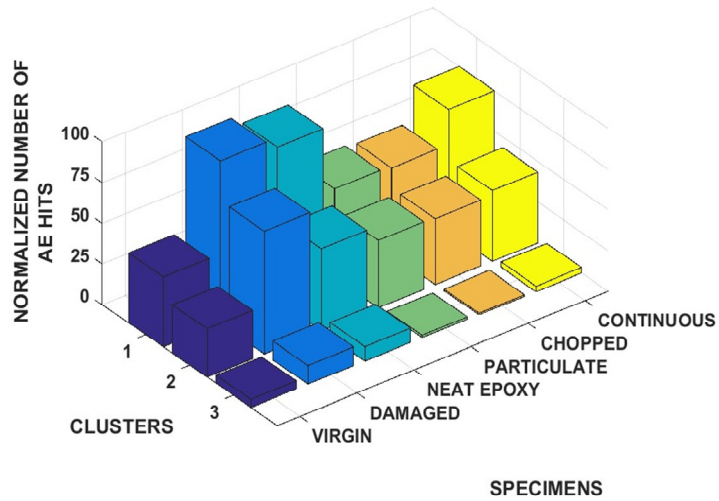Figure 12: Close up photographs of different failure modes in the glass/epoxy specimens.

Figure 13: Normalized number of AE hits versus clusters of virgin, damaged (notched) and
different repaired glass/epoxy specimens.

Table Captions:

Table 1: Summary of cluster results in the literature

Table 2: Properties of unidirectional glass fibers.

Table 3: Properties of epoxy araldite epoxy resin (LY556).

Table 4: Specification of AE sensor

Table 5: Compression behaviour of different repaired specimens

Table 6: Cluster validity evaluations for different specimens.

Table 1: Summary of cluster results in the literature

Authors	Matrix cracking	Debonding/delamination	Fiber breakage
Barre [29]	40-50 dB	60–65 dB	85–95 dB
Wadim [25]	30-45 dB	45– 55 dB	> 55 dB
Gong et al. [26]	33–45 dB	46 – 86 dB	87–100 dB
Kotsikos [28]	40–55 dB	55–70 dB	>80 dB
Kim and Lee [27]	40–70 dB	-	60–100 dB

Table 2: Properties of unidirectional glass fibers.

Properties	Standard	Specification	Tolerance	Units
Style Number	92145	/ FK100		
Weave Pattern	Plain	(DIN ISO 9354)		
Area weight of the weave pattern	220.0	DIN ISO 9354	± 5%	g/m^2
warp yarn		EC9-68x5 t0		
weft yarn		EC7-22		
Fiber count	1	DIN EN 1049		/ cm
Compression strength	510	DIN 65380	± 10%	MPa
Compression-Modulus	28		± 10%	GPa
Thickness (approx. dry)	0.25	DIN ISO 4603/E	± 5%	mm

In laminate (43% Vol.)	0.19		± 5%	mm

Table 3: Properties of epoxy araldite epoxy resin (LY556).

Properties	Standard	Units
Aspect (visual)	clear, pale yellow liquid	
Epoxy content (ISO 3000)	5.30 - 5.45	[eq/kg]
Viscosity at 25 °C (ISO 9371B)	10000 - 12000	[mPa s]
Flash point (ISO 2719)	> 200	[°C]
Density at 25 °C (ISO 1675)	1.15 - 1.20	[g/cm^3]

Table 4: Specification of AE sensor

Sensors Model	Picture	Dimensions OD X H (mm)	Weight (g)	Operating Temperature (^{0}c)	Materials		Operating Frequency Range (kHz)
					Case	Face	
WD (Wide Band)		18 × 17	20	-65 to 177	Stainless steel	Ceramic	100 - 900

Table 5: Compression behaviour of different repaired specimens

Specimens	Ultimate Load (kN)	Stiffness (kN/mm)
Virgin	64.60±0.493	24.35±0.364
Damaged	39.30±0.524	17.93±0.625
Neat Epoxy	46.00±1.094	18.98±0.459
Particulate	53.50±1.180	20.99±0.390
Chopped	54.80±0.943	22.83±0.696
Continuous	52.40±0.743	19.75±0.483

Table 6: Cluster validity evaluations for different specimens.

Specimens	Davies–Bouldin index	Silhouette coefficient
Virgin	0.6886	0.6682
Damaged	0.6942	0.6246
Neat Epoxy	0.7235	0.6724
Particulate	0.7604	0.6059
Chopped	0.6859	0.6590
Continuous	0.6445	0.6248